An Improved Analytical Model for the Elastic Constants of Auxetic and Conventional Hexagonal Honeycombs

Joseph N. Grima, Daphne Attard, Brian Ellul and Ruben Gatt

Metamaterials Unit, Faculty of Science, University of Malta, Msida, MSD 2080, Malta

Received: 14 April 2011, Accepted: 3 November 2011

SUMMARY

Cellular solids, in particular hexagonal honeycombs have been the subject of numerous studies in the last decades in view of their extensive use in many applications. In particular, there have been various studies aimed at expressing the mechanical properties of honeycombs in terms of the geometrical parameters used to describe the structure of such honeycombs. Despite improvements over the first established model, finite element simulations performed in this work on honeycombs having ribs with a realistic thickness-to-length ratio suggest that the mechanical properties for such systems differ from those predicted by current models, sometimes to a very significant extent. In view of this, we analyse in detail the deformed structures in an attempt to gain insight into how and the extent to which the shape of the ligaments, in particular its thickness and mode of connection affects deformation in conventional and re-entrant hexagonal honeycombs. Based on these observations, we propose a modified version of the previous analytical models that take into consideration the finite thickness of the ligaments.

INTRODUCTION

With a growing demand for new superior materials, in the last decades there has been an increasing interest in novel materials with an improved performance over the more traditional ones such as steel, wood or concrete. In particular, there were significant developments in cellular materials in view

of their exceptional strength-to-weight ratio [1]. A class of materials which is also attracting more attention is that of auxetic materials, i.e. materials with a negative Poisson's ratio, particularly auxetic cellular solids, such as auxetic foams [2-10] or auxetic honeycomb structures [11-28]. Such materials exhibit some very interesting properties ranging from improved indentation resistance to enhanced vibration absorption properties [29-36].

Over the years, several cellular systems [1-28,37-39], including ones which can lead to negative Poisson's ratios have been developed [2-28], the most well known being the classical two dimensional re-entrant and non re-entrant hexagonal honeycombs (see **Figure 1**) deforming primarily through flexure of the ribs. Such systems have been extensively modelled by Gibson and Ashby in their seminal 1982 work [11] where it has been proposed that for loading in the Ox_i direction, their on-axis Poisson's ratios ν^f_{ij} in the $Ox_i - Ox_j$ plane and Young's moduli E^f_i are given by:

$$\nu^f_{21} = \frac{1}{\nu^f_{12}} = \frac{\left[h/l + \sin(\theta)\right]\sin(\theta)}{\cos^2(\theta)} \tag{1}$$

$$E^f_1 = E_s\left(\frac{t}{l}\right)^3 \frac{\cos(\theta)}{\left[h/l + \sin(\theta)\right]\sin^2(\theta)} \quad E^f_2 = E_s\left(\frac{t}{l}\right)^3 \frac{h/l + \sin(\theta)}{\cos^3(\theta)} \tag{2}$$

where h, l and θ are geometric variables defined in **Figure 1** and E_s is the intrinsic Young's modulus of the material of the honeycomb. (The superscript 'f' denotes the mode of deformation, in this case flexure of the ribs.) Such systems have also been modelled by other workers including Evans et al. [13-16] who proposed that these honeycombs can deform through three non-mutually exclusive deformation mechanisms namely flexure of the ribs (Gibson and Ashby's model), stretching of the ribs (a property which is known to be particularly pertinent in some systems, for example in triangular lattices or in particular conformations of hexagonal honeycombs) and/or hinging of the ribs. In view of this, Evans et al. have further extended the flexure model to include hinging and stretching [13-14] with the Young's moduli and Poisson's ratios of systems deforming through concurrent flexure, hinging and stretching being given by:

$$E_i^{f+s+h} = \left(\frac{1}{E_i^f} + \frac{1}{E_i^s} + \frac{1}{E_i^h}\right)^{-1} \tag{3}$$

$$\nu_{ij}^{f+s+h} = -E_i^{f+s+h}\left(\frac{-\nu_{ij}^{f}}{E_i^{f}} + \frac{-\nu_{ij}^{s}}{E_i^{s}} + \frac{-\nu_{ij}^{h}}{E_i^{h}}\right) \tag{4}$$

where E^f_i, E^s_i and E^h_i are the Young's moduli for loading in the Ox_i direction due to flexing, stretching and hinging respectively whilst ν^f_{ij}, ν^s_{ij} and ν^h_{ij} are the Poisson's ratios in the $Ox_i - Ox_j$ plane for loading in the Ox_i direction due to flexing, stretching and hinging respectively which are given by:

Idealised Stretching model:

$$\nu_{21}^{s} = -\frac{\sin(\theta)\left(h/l+\sin(\theta)\right)}{2h/l+\sin^2(\theta)} \quad \nu_{12}^{s} = -\frac{\sin(\theta)}{\sin(\theta)+h/l} \tag{5}$$

$$E_1^{s} = \frac{K_s}{b\cos(\theta)\left(h/l+\sin(\theta)\right)} \quad E_2^{s} = \frac{K_s\left(h/l+\sin(\theta)\right)}{b\cos(\theta)\left(2h/l+\sin(\theta)\right)} \tag{6}$$

Idealised Hinging model:

$$\nu_{21}^{h} = \frac{1}{\nu_{12}^{h}} = \frac{\sin(\theta)\left(h/l+\sin(\theta)\right)}{\cos^2(\theta)} \tag{7}$$

$$E_1^{h} = \frac{K_h\cos(\theta)}{b\sin^2(\theta)\left(h/l+\sin(\theta)\right)} \quad E_2^{h} = \frac{K_h\left(h/l+\sin(\theta)\right)}{b\cos^3(\theta)} \tag{8}$$

where b is the thickness of the honeycomb in the third direction, K_s and K_h are the stretching and hinging force constants being given by:

$$K_s = \frac{btE_s}{l}\ ;\ K_h = \frac{G_s bt}{l} \tag{9}$$

where G_s is the shear modulus of the material making up the honeycomb given by $E_s/2(1+n)$ if the material is isotropic. Note that Masters and Evans also re-express the equations for the Young's moduli derived by Gibson and Ashby in terms of a flexure stiffness constant K_f as:

$$E_1^f = \frac{K_f \cos(\theta)}{b\left[h/l + \sin(\theta)\right]\sin^2(\theta)} \quad E_2^f = \frac{K_f \left[h/l + \sin(\theta)\right]}{b\cos^3(\theta)} \tag{10}$$

where K_f is defined by :

$$K_f = \frac{E_s b t^3}{l^3} \tag{11}$$

Although the analytical model derived by Masters and Evans provides a more accurate representation of real honeycombs when compared to that derived by Gibson and Ashby, for example, it has been shown that they are more suitable for modelling of molecular level honeycombs built using phenyl rings and acetylene chains, both models may not take into account some consequences that may arise from having ribs of a finite non-negligible thickness. In particular, while the models have the advantage of being highly elegant and, as shall be shown further on, suitable for modelling honeycombs having very slender ribs or very particular junctions, they may not be accurate enough to predict the mechanical properties of some real honeycombs. In view of this, in this work, we use the finite element (FE) method to model both conventional and re-entrant configurations of these hexagonal honeycombs using beam elements as well as plane elements which are likely to offer a much more faithful representation of real systems. The simulation results are then compared with the analytical models, to quantify by how much they

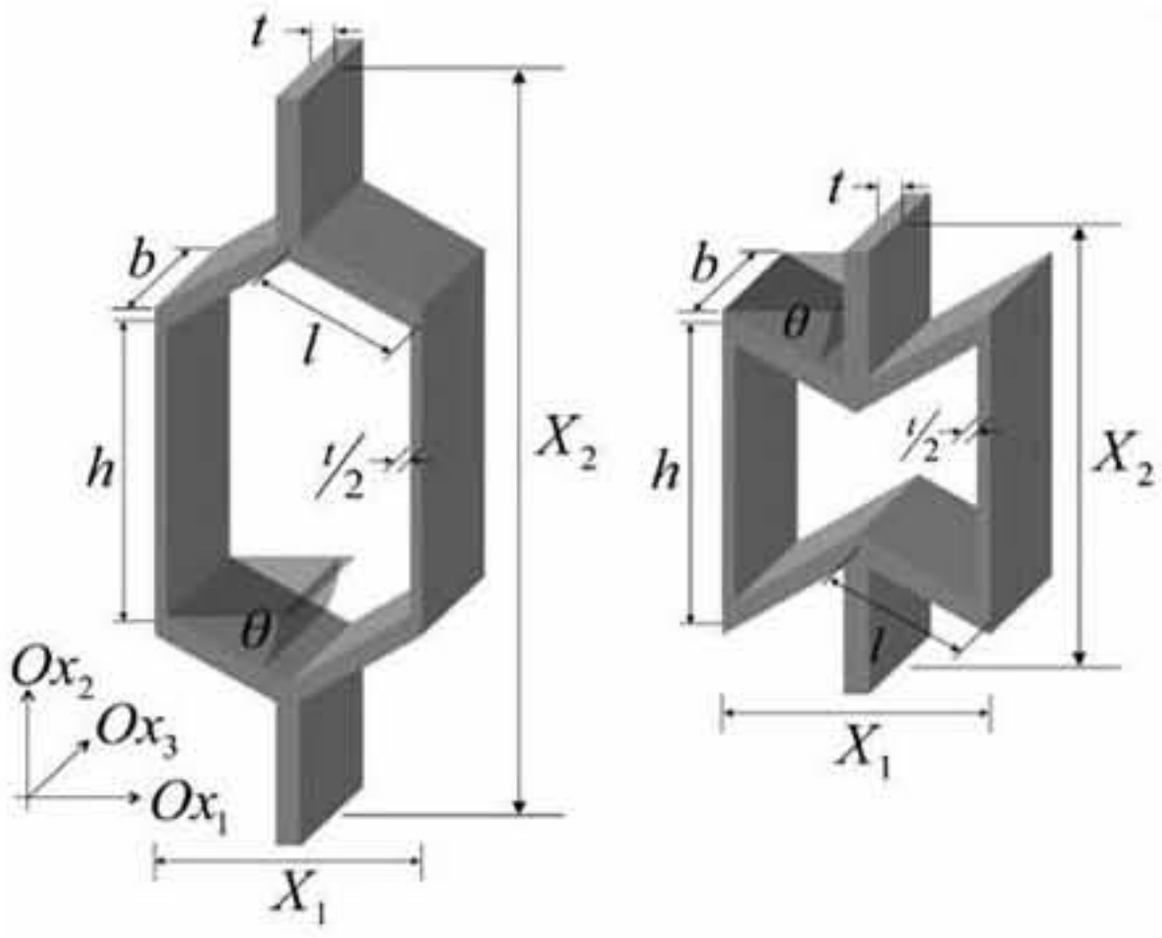

Figure 1. *Geometry of (a) conventional (non re-entrant) and (b) re-entrant hexagonal honeycombs*

deviate from real systems. The results are also used in attempt to provide an improved analytical model which takes into account the main shortcomings in existing models based on a similar simple beam theory approach to retain much of the simplicity and form of the original models.

2. SIMULATIONS

Two sets of numerical simulations were carried out using the commercial finite element software ANSYS® Academic Research, Release 12.0 on honeycombs having the rib lengths h and l set to 20 and 10 respectively while the angle θ was varied between -60° and +60°. In the first set the honeycomb were constructed from 'beam elements' representing the ribs, whilst in the second set, the honeycombs were constructed using 'plane elements'.

In the simulations using beam elements, the beams were set to have a rectangular cross-section of dimensions t × z where t is the thickness in the xy-plane having a value in the range 0.1-1.0 and z is the depth in the third direction which was set to 1. In an attempt to obtain simulations which represent as much as possible the scenario suggested by Gibson et al. (1982), where the beam is considered to deform solely in the plane of the structure (deformations only in xy-plane), any translations in the z-direction and rotations in the x- and y-directions were restricted. The remaining boundary conditions (BCs) were set to simulate periodicity. The material was modelled as an isotropic and perfectly elastic one with a Young's modulus of E_s= 10 GPa and a typical Poisson's ratio of ν_s= 0.3. Following a mesh sensitivity analysis, the honeycombs' geometries were meshed using the 3D, 2-noded, BEAM188 element which utilises the Timoshenko beam formulation. This means that deformations due to shear are taken into account therefore it is suitable for analysing slender to moderately thick beam structures.

In the case of the plane element analysis, the 2D 8-Node PLANE82 with plane strain element behaviour was used. Taking advantage of the symmetry of the unit cell for such honeycombs and applying the correct boundary conditions to simulate periodicity (as shown in **Figure 2**), an infinite planar hhoneycomb network was modelled using a quarter of the unit cell. The lengths of the inclined and vertical ribs measured halfway through the thickness t were set as l and h respectively. The same geometric parameters used in the simulations for the beam elements were used.

For both sets of simulations, the Young's moduli were then calculated by measuring the total reaction force $\sum F_i$ in the loading direction on the nodes on which the displacement was applied and dividing by $A_i e$, where A_i is the area of the face of the unit cell normal to the direction of loading and ε is the

strain applied (= 0.05). The Poisson's ratios were calculated by measuring the displacement of the nodes lying on the face that is free to move in the direction orthogonal to the loading direction and dividing by the applied strain.

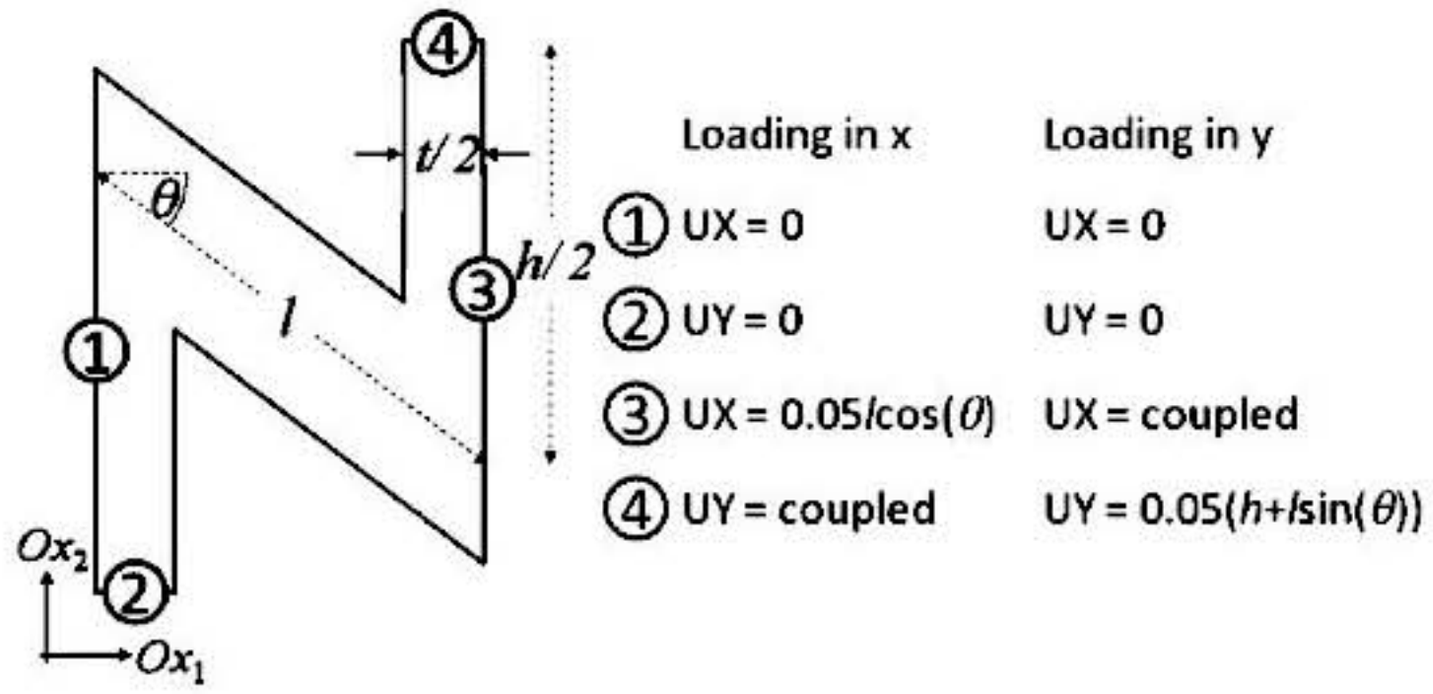

Figure 2. *Boundary conditions applied for plane element analysis of the honeycombs*

Figures 3 and **4** show plots for the variation of the Young's moduli and Poisson's ratios with the angle θ as predicted by the FE methods and the existent analytical models for honeycombs having different rib thickness t, and with h = 20 mm and l = 10 mm. From these plots, it is evident that the predictions of the moduli made from the FE simulations using beam elements differ from those obtained using plane elements, in some cases by as much as 60%. This phenomenon was previously overlooked and clearly indicates that any model of honeycombs based on beam theory may need to be checked so as to establish whether it can adequately model real honeycomb systems such as those produced using rapid prototyping techniques. In fact, here it should be noted that the FE beam model is actually simulating a scenario where the three beams which meet at a single joint, two of length l and one of length h, are in reality located in different spatial position and do not intersect, something which is highly unrealistic.

The simulations also suggest that the flexure model derived by Gibson and Ashby provides a good estimate of the properties of most, but not all honeycombs simulated using beam elements. This is very significant as it confirms the suitability of Gibson and Ashby's model for predicting the behaviour of real systems. However, the model derived by Evans et al. for concurrent deformation appears to be more general in the sense that it provides a better fit to the results obtained from the FE simulations using beam elements, including honeycombs made from beam elements which could not be modelled effectively by Gisbon and Ashby's model (e.g. loading of honeycombs in the Ox_1 directions where θ tends to 0° where obviously the stretching mechanism is the dominant mechanism). This shows that the

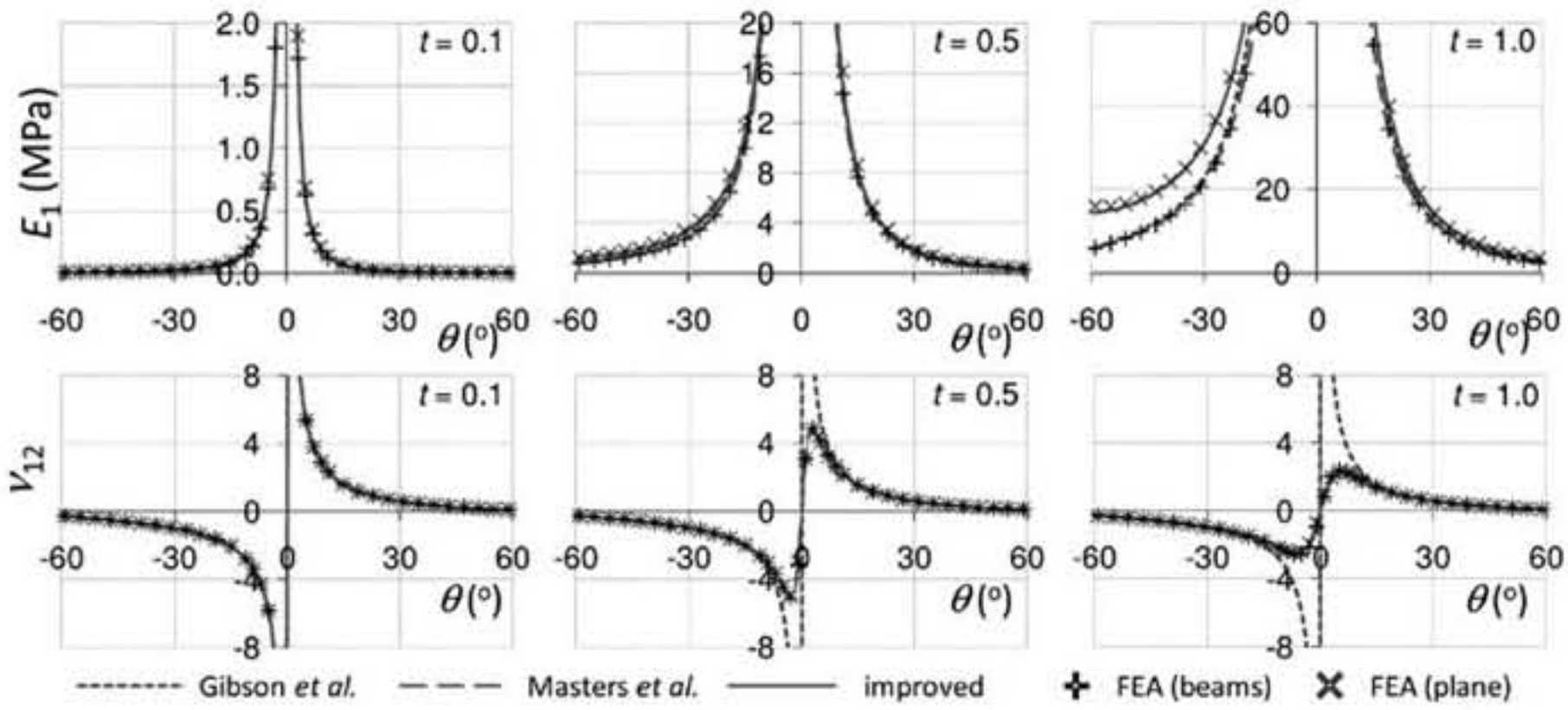

Figure 3. *Variation for the Young's modulus and Poisson's ratios for conventional (θ>0) and auxetic honeycombs (θ<0) for loading in the Ox_1-direction*

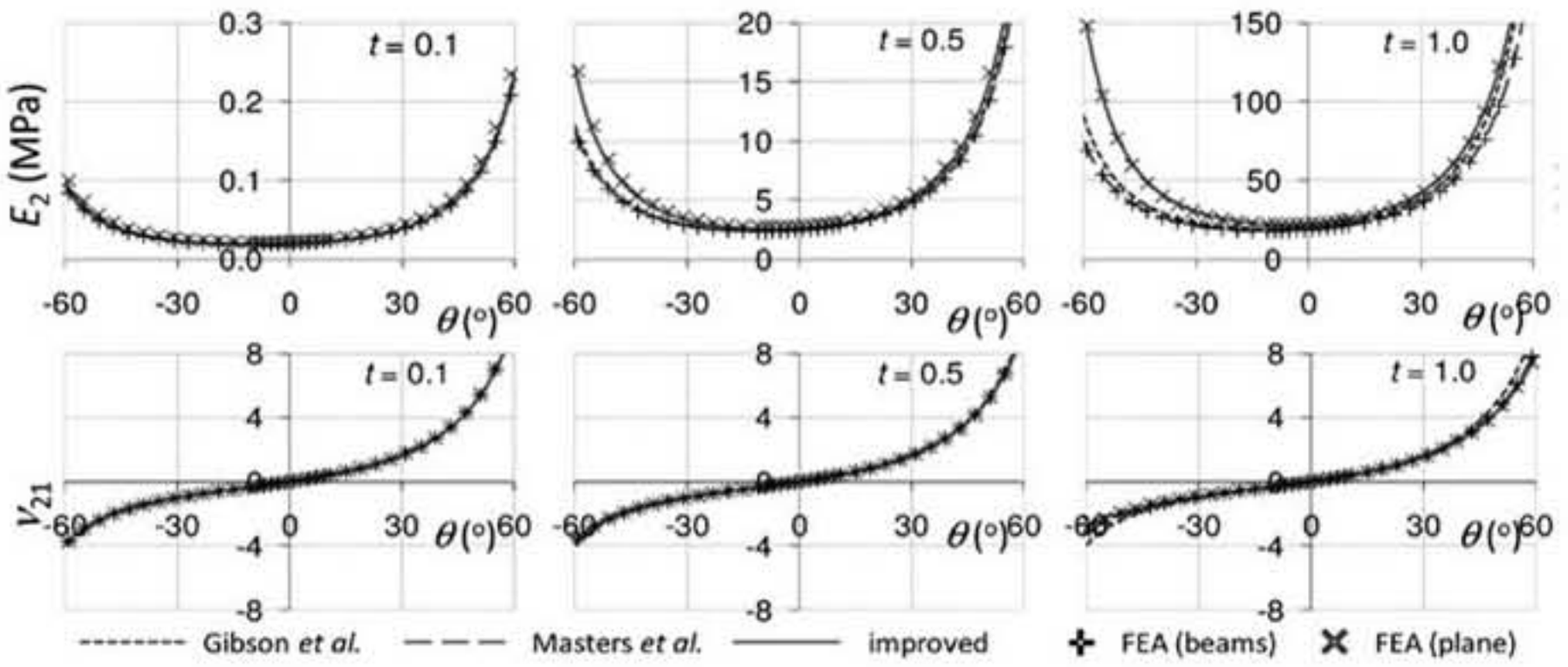

Figure 4. *Variation for the Young's modulus and Poisson's ratios for conventional (θ>0) and auxetic honeycombs (θ<0) for loading in the Ox_2-direction*

combined Gibson et al.–Evans et al. models, henceforth referred to as the idealised model, is more accurate at predicting the mechanical properties than any single mode deformation model.

However, even this model fails to adequately predict some of the results obtained from FE simulations using plane elements, which deviations are most pronounced for the Young's modulus but not as much for the Poisson's ratio. This deviation in the moduli is to be expected given that the results of the FE simulations obtained using beam elements and those obtained using plane elements do not agree between themselves in the prediction of the moduli. Our results also suggest that these deviations become more significant at large magnitudes of the angle θ, and are more pronounced in

re-entrant configurations. In particular, it is evident that the analytical model always underestimates the true values of the Young's moduli. This suggests that the extent of deformation of the ribs in real systems is somewhat lower than that which is assumed in the analytical models.

These deviations may be explained by the fact that if these honeycombs are analysed carefully, one may note that there is a region (region 1 in **Figure 5**) which is considered by the idealised model but in real honeycombs is spatially incorporated within the other ribs and outside the unit cell boundary used in the derivation of the model. In both the conventional and auxetic honeycombs, this region increases with thickness and magnitude of the angle. There is also a second region of overlap between the vertical and inclined ribs (region 2 in **Figure 5**). This results in a mass of material at the joint which inhibits deformation from occurring along the whole of length l, an effect which becomes more and more pronounced as the thickness increases. This effect is much more prominent in re-entrant honeycombs than in conventional ones due to the much larger degree of overlap which increases as the magnitude of the angle θ increases as opposed to conventional honeycombs where degree of overlap becomes smaller for the larger angles. The hypothesis that these regions are an important cause in the deviations between the analytical model and the properties of realistic honeycombs is corroborated by the fact that our FE simulations suggest that larger deviations occur for negative values of θ and much smaller deviations for positive values, as evident from the graphs in **Figures 3** and **4**. Consequently, by considering all of length l in ideal models, one is incorrectly assuming that these regions are deforming to their full potential, and therefore that for an applied stress more energy is stored than actually is so that the resulting Young's modulus is lower than the actual. Thus, when analysing the deformations of such honeycombs, it may be more realistic to consider an effective length l_{eff} for the ribs, which is slightly shorter

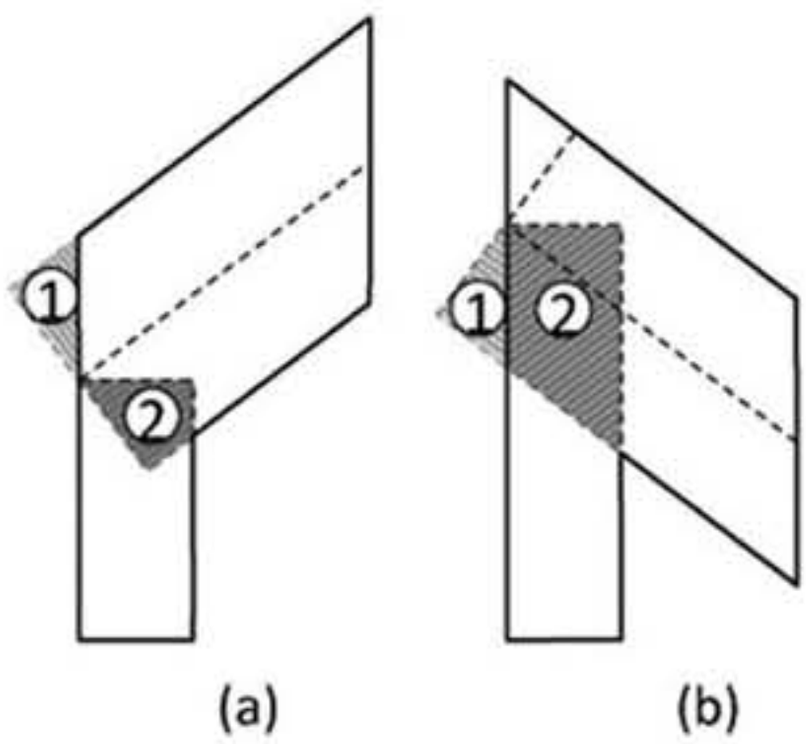

Figure 5. *Overlapping regions of the vertical and inclined ribs in (a) conventional and (b) auxetic honeycombs which occur in real systems as a result of their rib thickness. Note that region 1 does not form part of the unit cell*

than the actual length l and along which the actual deformations occur. This hypothesis will form the basis of our improved model presented in **Figure 5**.

3. IMPROVED ANALYTICAL MODEL

In view of the results of the simulations, a new set of expressions is being proposed for the Young's moduli and Poisson's ratios of hexagonal honeycombs where some of the dimensional parameters in the idealised models derived by Gibson et al. and Evans et al. are replaced by more realistic effective parameters.

3.1 Idealised Flexure Model

Referring back to **Figure 1**, as discussed elsewhere [11-14], the honeycomb structure may be defined in terms of a rectangular unit cell having dimensions X_1 and X_2 in the Ox_1 and Ox_2 directions respectively and a thickness b in the third direction Ox_3 where X_1 and X_2 are respectively given by:

$$X_1 = 2\left[h + l\sin(\theta)\right] \tag{12}$$

$$X_2 = 2\cos(\theta) \tag{13}$$

Referring to **Figure 6**, in analogy to earlier work [11-12], a stress s_1 in the Ox_1 direction results in flexure of slanting cell ligaments as a result of the force P acting on the ligaments in the Ox_1 direction given by:

$$P = \frac{1}{2}\sigma_1 X_2 b \tag{14}$$

This force will generate a moment under which the ligaments tend to bend. For the purpose of this derivation these ligaments are treated as a beam of length l, part of which does not flex as it is embedded within the joint of the honeycomb. Thus, the deformable part of the ligament only has an effective length l_{eff} an in-plane and out-of-plane thickness of t and b respectively and an intrinsic Young's modulus of E_s. Then from standard beam theory the resulting ligament deflection is given by [40]:

$$\delta^f = \frac{P l_{eff}^3 \sin(\theta)}{12 E_s I} \tag{15}$$

where I is the second moment of inertia of the ligament which for beams having a rectangular cross-sectional area is given by:

$$I = \frac{bt^3}{12} \tag{16}$$

The strains in the Ox_1 and Ox_2 direction are given by:

$$\varepsilon_1^f = \frac{2\delta^f \sin(\theta)}{X_1} \tag{17}$$

and:

$$\varepsilon_2^f = -\frac{2\delta^f \cos(\theta)}{X_2} \tag{18}$$

which means that the Poisson's ratio for loading in the Ox_1 direction is given by:

$$\nu_{12}^f = -\frac{\varepsilon_2}{\varepsilon_1} = \frac{X_1}{X_2}\cot(\theta) \tag{19}$$

which is the same expression as that derived by Gibson and Ashby whilst the Young's modulus in the Ox_1 direction is given by:

$$E_1^f = \frac{\sigma_1}{\varepsilon_1} = E_s \frac{X_1}{X_2}\left(\frac{t}{l_{eff}}\right)^3 \frac{1}{\sin^2(\theta)} \tag{20}$$

In analogy to the work by Masters and Evans, this Young's modulus may be expressed in terms of K_f', the flexure force constant as:

$$E_1^f = \frac{\sigma_1}{\varepsilon_1} = \frac{K_f'}{b}\frac{X_1}{X_2}\frac{1}{\sin^2(\theta)} \tag{21}$$

where K_f' is given by:

$$K_f' = \frac{E_s bt^3}{l_{eff}^3} \tag{22}$$

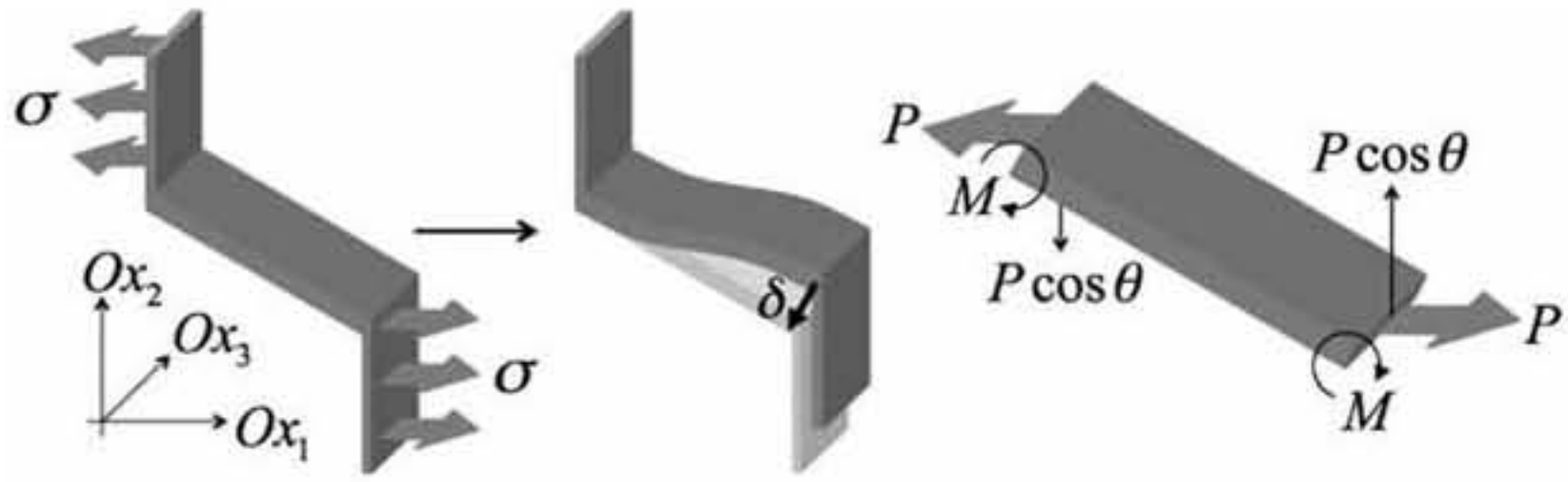

Figure 6. *(a) Deformation of a cell wall through the flexure mechanism and (b) a free-body diagram of the deforming inclined rib*

Similarly, for loading in the Ox_2 direction, the Poisson's ratios ratio (which are the same as those derived by Gibson and Ashby) and the Young's moduli are given by:

$$\nu_{21}^{f} = -\frac{\varepsilon_1}{\varepsilon_2} = \frac{X_2}{X_1}\tan\left(\theta\right) \tag{23}$$

and:

$$E_2^f = \frac{\sigma_2}{\varepsilon_2} = E_s \frac{X_2}{X_1}\left(\frac{t}{l_{eff}}\right)^3 \frac{1}{\cos^2\left(\theta\right)} = \frac{K_f'}{b}\frac{X_2}{X_1}\frac{1}{\cos^2\left(\theta\right)} \tag{24}$$

3.2 Idealised Stretching Model

A similar approach can also be used to modify the equations for the idealized stretching model. In fact, in analogy to the above, it may be argued that deformations resulting from stretching of the ligaments will be much more pronounced in the portion between the joints than in the joints themselves so that once again, it may be more realistic to consider that portion of the ligament of length l_{eff} (which can be assumed to be the same l_{eff} as that used in the flexing model) rather than the whole length l. In this way, applying Hooke's law, the extension along the ligament can be expressed as:

$$\delta^s = \frac{Pl_{eff}\cos\left(\theta\right)}{E_s bt} = \frac{P\cos\left(\theta\right)}{K_s'} \tag{25}$$

where

$$K_s' = \frac{E_s bt}{l_{eff}} \tag{26}$$

The resulting strains in the Ox_1 and Ox_2 directions are respectively given by:

$$\varepsilon_1^s = \frac{2\delta^s \cos(\theta)}{X_1} \text{ and } \varepsilon_2^s = \frac{2\delta^s \sin(\theta)}{X_2} \tag{27}$$

so that for loading in the Ox_1 direction, the Poisson's ratio can be given by:

$$\nu_{12}^s = -\frac{\varepsilon_2}{\varepsilon_1} = -\frac{X_1}{X_2}\tan(\theta) \tag{28}$$

and the Young's modulus by:

$$E_1^s = \frac{\sigma_1}{\varepsilon_1^s} = \frac{K_s'}{b}\frac{X_1}{X_2}\frac{1}{\cos^2(\theta)} \tag{29}$$

A similar approach can also be used to modify the equations for loading in the y-direction. However in this case, it should be noted that the vertical ribs may deform by stretching so their effective length, which is denoted by h_{eff}, must also be considered. Therefore, the stretching force constant for ribs of length h can be rewritten as:

$$K_s^{[h]} = \frac{E_s bt}{h_{eff}} \tag{30}$$

which can be related to the stretching force constant $K_s¢$ for the rib of length l_{eff} as follows:

$$K_s^{[h]} = \frac{K_s' l_{eff}}{h_{eff}} \tag{31}$$

Thus for loading in the Ox_2 direction, the expression for the in-plane Poisson's ratio is given by:

$$\nu_{21}^{s} = -\frac{X_2}{X_1}\frac{\sin(\theta)\cos(\theta)}{\sin^2(\theta)+2h_{eff}/l_{eff}} \tag{32}$$

while that for the Young's modulus is given by:

$$E_2^{s} = \frac{K_s'}{b}\frac{X_2}{X_1}\frac{1}{\sin^2(\theta)+2h_{eff}/l_{eff}} \tag{33}$$

3.3 Idealised Hinging Model

In analogy to Masters and Evans's model, one may also derive a set of expressions for such honeycombs where one assumes that the deformation is concentrated at the joints. The expressions for such idealized hinging model would be of the same form as those derived in the idealized flexure model with the difference that the flexure force constant will be replaced by a hinging force-constant which is given by:

$$K_h' = \frac{E_s bt}{2(1+\nu)l_{eff}} \tag{34}$$

i.e. the Poisson's ratios and Young's moduli for the idealized hinging models are given by:

$$\nu_{12}^{h} = \frac{1}{\nu_{21}^{h}} = -\frac{\varepsilon_1}{\varepsilon_2} = \frac{X_1}{X_2}\cot(\theta) \tag{35}$$

$$E_1^{h} = \frac{\sigma_1}{\varepsilon_1} = \frac{K_h'}{b}\frac{X_1}{X_2}\frac{1}{\sin^2(\theta)} \tag{36}$$

and:

$$E_2^{h} = \frac{\sigma_2}{\varepsilon_2} = \frac{K_h'}{b}\frac{X_2}{X_1}\frac{1}{\cos^2(\theta)} \tag{37}$$

3.4 Combined Flexure, Hinging and Stretching Model

Using equations 3-4, the expressions for the Poisson's ratios and Young's moduli for a model which deforms through concurrent flexure, hinging and stretching for loading in the Ox_1 direction, can be written as:

$$\nu_{12} = \frac{\sin(\theta)\cos^2(\theta)\left[\left(l_{eff}/t\right)^2 + 1 + 2\nu\right]}{\left[h/l + \sin(\theta)\right]\left[\left(l_{eff}\sin(\theta)/t\right)^2 + 2(1+\nu)\sin^2(\theta) + \cos^2(\theta)\right]} \tag{38}$$

$$E_1 = \frac{E_s t\cos(\theta)}{l_{eff}\left(h/l + \sin(\theta)\right)\left[\left(l_{eff}\sin(\theta)/t\right)^2 + 2(1+\nu)\sin^2(\theta) + \cos^2(\theta)\right]} \tag{39}$$

whilst for loading in the Ox_2 direction:

$$\nu_{21} = \frac{\sin(\theta)\left[h/l + \sin(\theta)\right]\left[1 + 2\nu + \left(l_{eff}/t\right)^2\right]}{\left[2h_{eff}/l_{eff} + \sin^2(\theta) + 2(1+\nu)\cos^2(\theta) + \left(l_{eff}\cos(\theta)/t\right)^2\right]} \tag{40}$$

$$E_2 = \frac{E_s t\left(h/l + \sin(\theta)\right)}{l_{eff}\cos(\theta)\left[\left(2h_{eff}/l_{eff} + \sin^2(\theta)\right) + \left(l_{eff}\cos(\theta)/t\right)^2 + 2(1+\nu)\cos^2(\theta)\right]} \tag{41}$$

Note that these expressions are equivalent to those that would have been obtained if the expressions of the force constants K_f¢, K_s¢ and K_h¢ derived here, i.e.:

$$K_f' = \frac{E_s bt^3}{l_{eff}^3};\ K_s' = \frac{btE_s}{l_{eff}};\ K_h' = \frac{E_s bt}{2(1+\nu)l_{eff}} \tag{42}$$

are substituted in the combined expressions for the Poisson's ratios and Young's moduli derived by Masters and Evans. Hoverer, it should noted that the geometric parameter l is not always being replaced by l_{eff} in the expressions as indicated in the derivation.

4. DISCUSSION

The expressions derived here clearly show that equations for the Young's moduli and Poisson's ratios based on the assumption that there is concurrent stretching; hinging and flexure are in the same overall format as those derived by other workers with the difference that in some cases, the effective lengths/heights (l_{eff}, h_{eff}) of the ligaments should replace the true geometric lengths/heights (l, h). It is however obvious that the success or otherwise of the newly derived equations to predict the true properties of real honeycombs will depend on the ability to correctly identify the correct values of l_{eff} and h_{eff} to be used instead of the true geometric dimensions.

In an attempt to establish a useful relationship between these effective dimensions and the geometry of the honeycomb, we analysed the deformation for several honeycombs, some of which are shown in **Figure 7**. Superposition of the deformed and undeformed structures as well as the stress intensity plots (**Figure 8**) suggest that deformations in the inclined ribs do not occur uniformly throughout the whole length l as predicted by the simple beam model. Instead, it appears that most of the deformation in the lower surface of the rib occurs outward from the junction that it forms with the inner surface of the

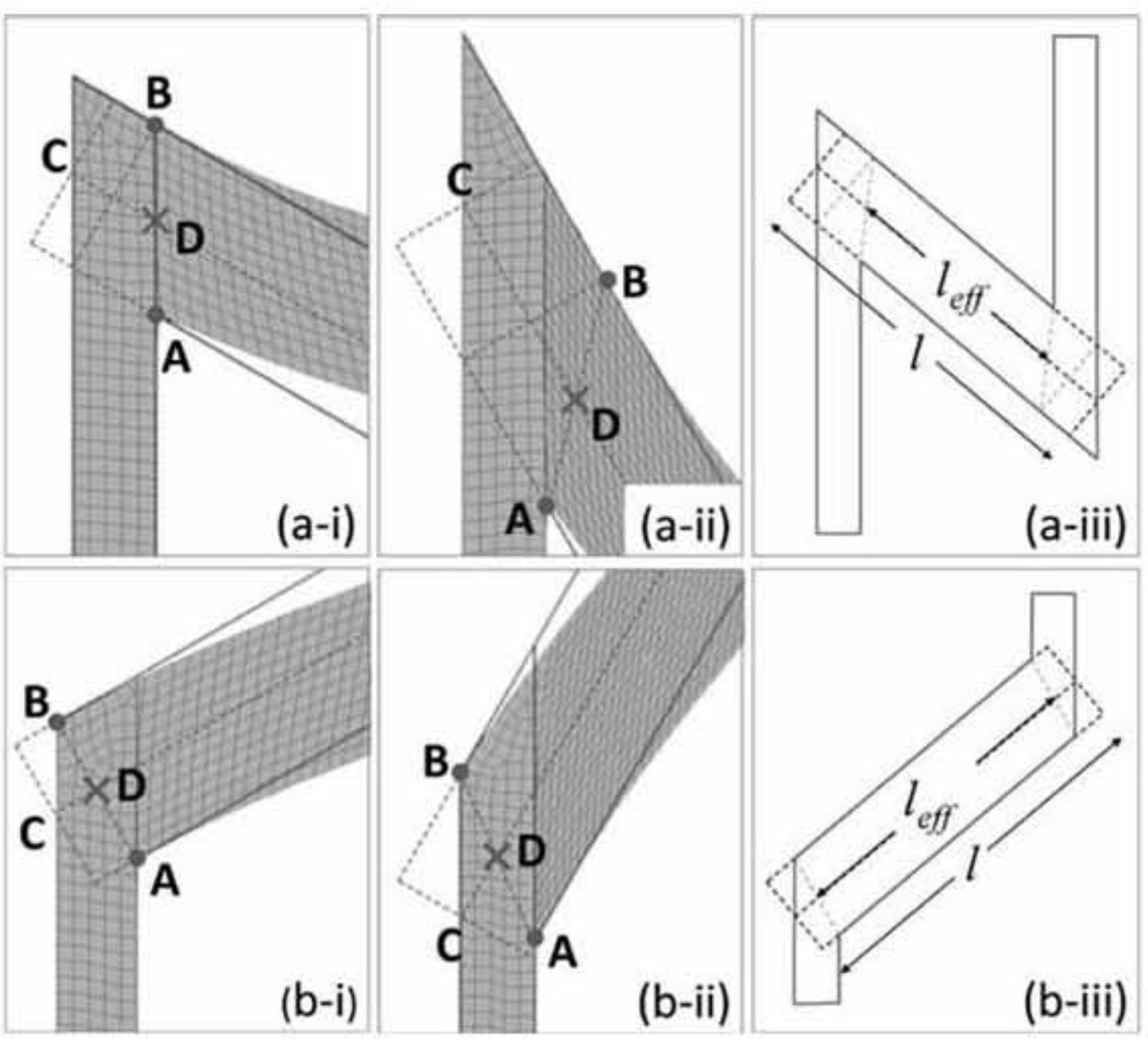

Figure 7. *Superposition of the deformed and undeformed structure for (a) auxetic and (b) conventional honeycombs at (i) |30°| and (ii) |60°| showing the point from where deformation in the inclined ribs is assumed occur when loaded in the Ox_1 direction*

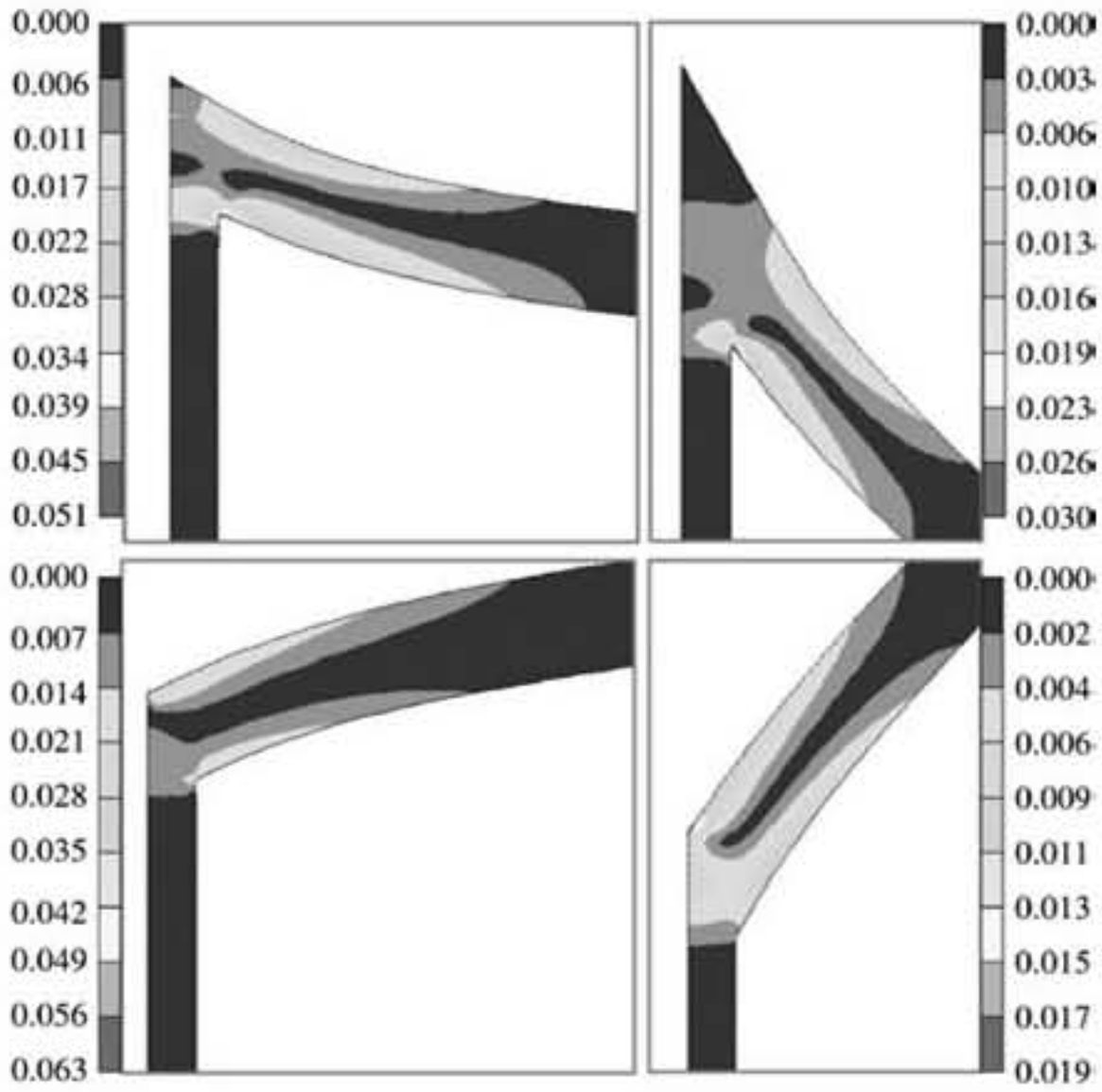

Figure 8. *Von Mises stress plots for the deformed structures shown in Figure 7*

vertical rib, indicated by point A. This effect is observed for both re-entrant and conventional honeycombs. Similarly, for conventional honeycombs, deformation along the opposite upper surface of the rib occurs mainly from the vertex at the junction formed with the vertical rib indicated by point B. For re-entrant honeycombs, there is no clear point from where deformation occurs. However, it has been observed to occur from near a point which can be related to the geometry of the honeycomb as shown in **Figure 7**. Thus, it is being proposed that a suitable point from where to measure the effective length would be one laying half way in between points A and B i.e. at the intersection between the neutral surface of the inclined rib and the line joining points A and B indicated by the location of the position D in **Figure 7**.

Thus, the effective length of the inclined ribs can in general be written as:

$$l_{eff} = l - 2l_{CD} \tag{43}$$

where using the same convention as that used by Gibson for the angle, i.e. positive values for conventional honeycombs and negative values for auxetic ones, then for non re-entrant honeycombs (see **Figure 9a**) the length l_{CD} is given by:

$$l_{CD} = \frac{t}{4}\left[\tan\left(\frac{\pi}{4} - \frac{\theta}{2}\right) + \tan(\theta)\right] \text{ where } 0 \le \theta < \frac{\pi}{2} \tag{44}$$

while for re-entrant honeycombs (**Figure 9b**) the length l_{CD} is given by:

$$l_{CD} = \frac{t}{4}\left[\tan\left(\frac{\pi}{4}-\frac{\theta}{2}\right)-\tan(\theta)\right] \text{ where } 0 \geq \theta \geq \theta_m \tag{45}$$

where θ_m is the bound which ensures that θ satisfies the condition that $h+2l\sin(\theta)-t\cos(\theta)>0$ in order to avoid any overlap of an inclined rib with the ones above or below it.

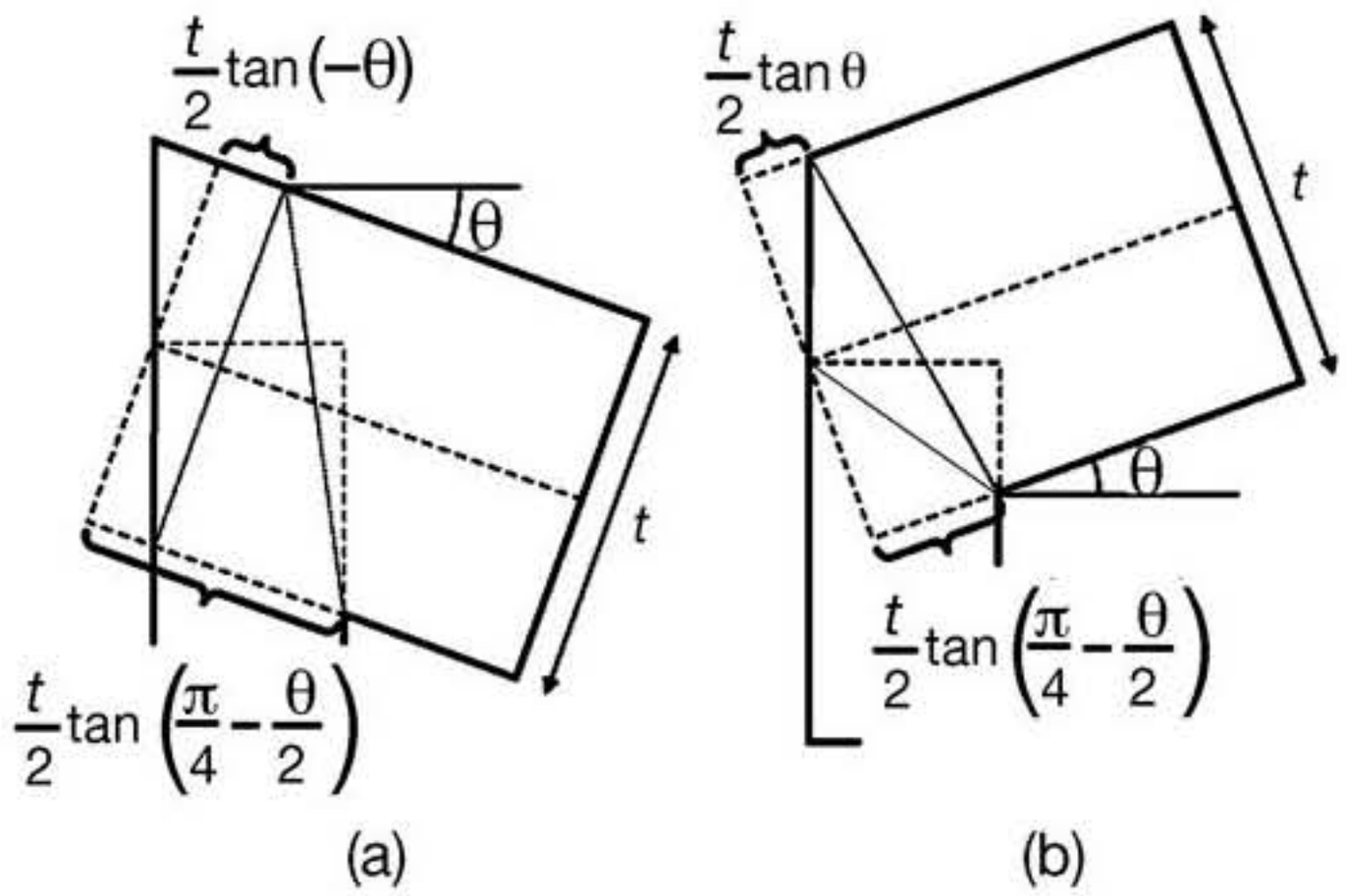

Figure 9. *Geometry relationships at the joint required to find the effective length*

Similarly, the plots of the internal stress in the y-direction (see **Figure 11**) suggest that deformation does not occur along the whole length h but along a length that is slightly smaller than h but slightly larger than that indicated by point A in **Figure 10**. Once again, a good approximation is to take the average of the two lengths indicated by point D such that the effective length is given by:

$$h_{eff} = h - 2l_{CD} = h - \frac{t}{2}\tan\left(\frac{\pi}{4}-\frac{\theta}{2}\right) \tag{46}$$

for both the conventional and auxetic honeycombs.

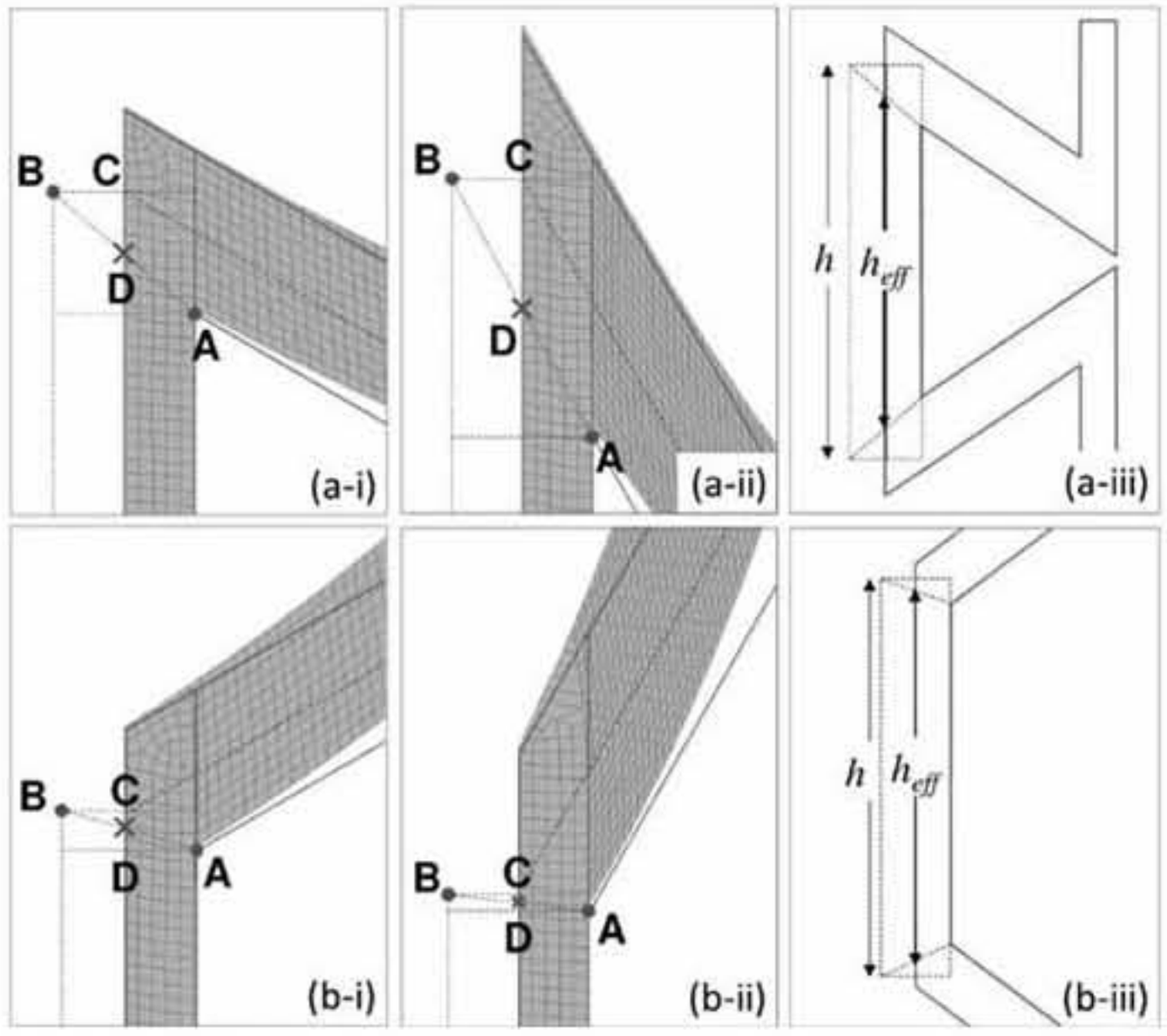

Figure 10. *Superposition of the deformed and undeformed structure for (a) auxetic and (b) conventional honeycombs at (i) \|30°\| and (ii) \|60°\| showing the point from where deformation in the vertical ribs is assumed to occur when loading in the Ox_2-direction*

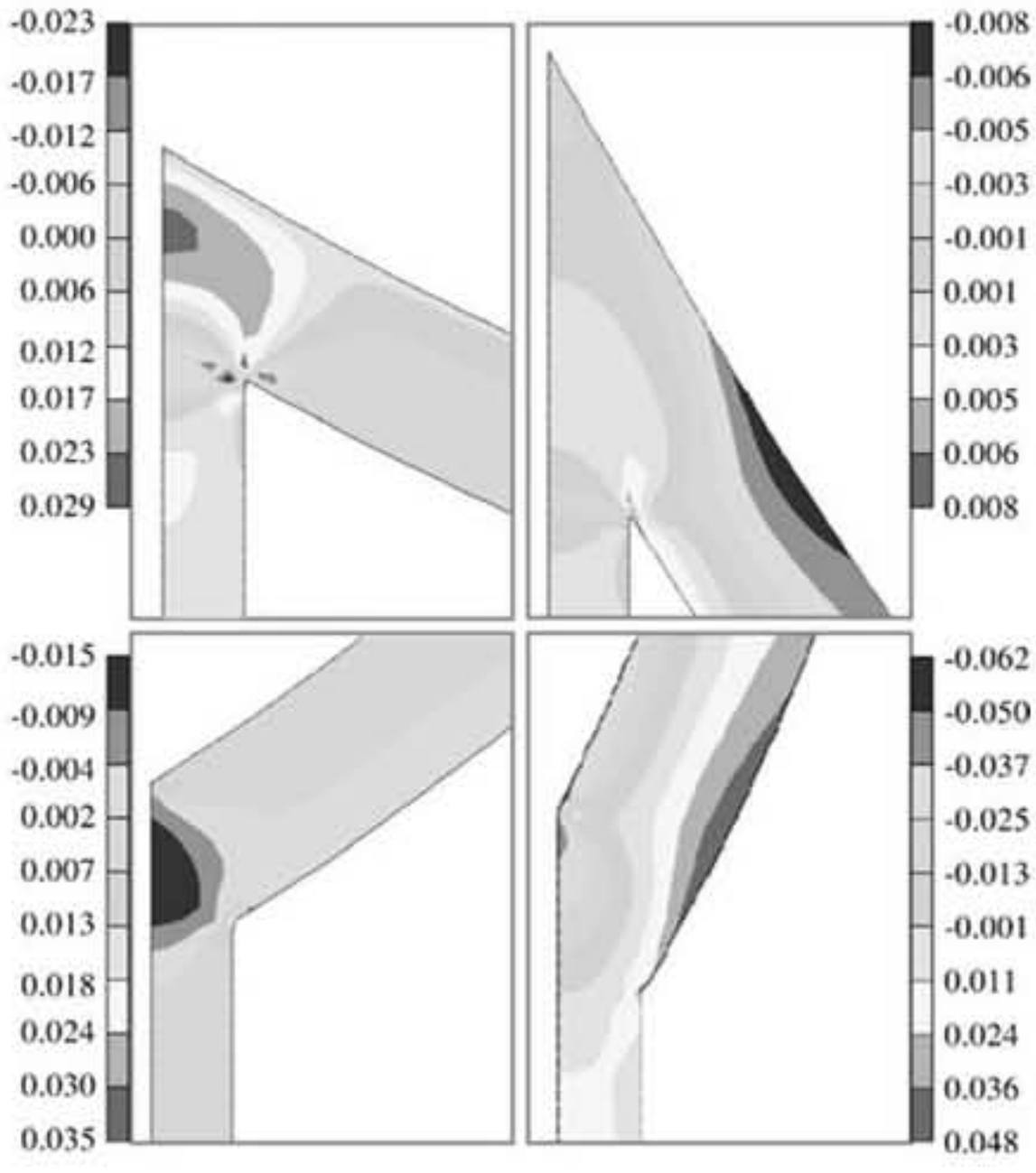

Figure 11. *Typical plots for the vertical (y)-component of the stresses in the vertical ribs*

Having established the proposed magnitudes for l_{eff} and h_{eff}, one may use the expressions 38-41 to examine their ability to predict the properties of honeycombs predicted by the FEA simulations as well as establish the deviations from the earlier analytical models.

As illustrated in the plots in **Figures 3-4**, a substitution of the proposed expressions for l_{eff} and h_{eff} into the expressions for the moduli and Poisson's ratios derived above suggest that there is a significant improvement in agreement with the results obtained from the FE plane elements simulations which is particularly evident for systems having large values of t. At low values of t, the new Young's modulus and Poisson's ratios are very similar to the published ones (see **Figure 12**), as expected, i.e. the corrections to the Gibson et al. and Masters et al. models are most pertinent if the ribs are relatively thick Here it should be noted that, as t increases, the discrepancy between the values predicted by the new and the published models increases considerably, and although the results of the simulations suggest that our models are valid to model systems with non insignificant t/l ratios, care should be taken to ensure that the thickness to length ratios used are still such that they permit the use of the Euler-Bernoulli beam theory. In particular, it should be noted that our derivation is based on the assumption that only part of the ligament is behaving as a beam, and one must ensure that the ratio l_{eff}:t is large enough to permit the assumption to remain valid, and not l:t. In fact,

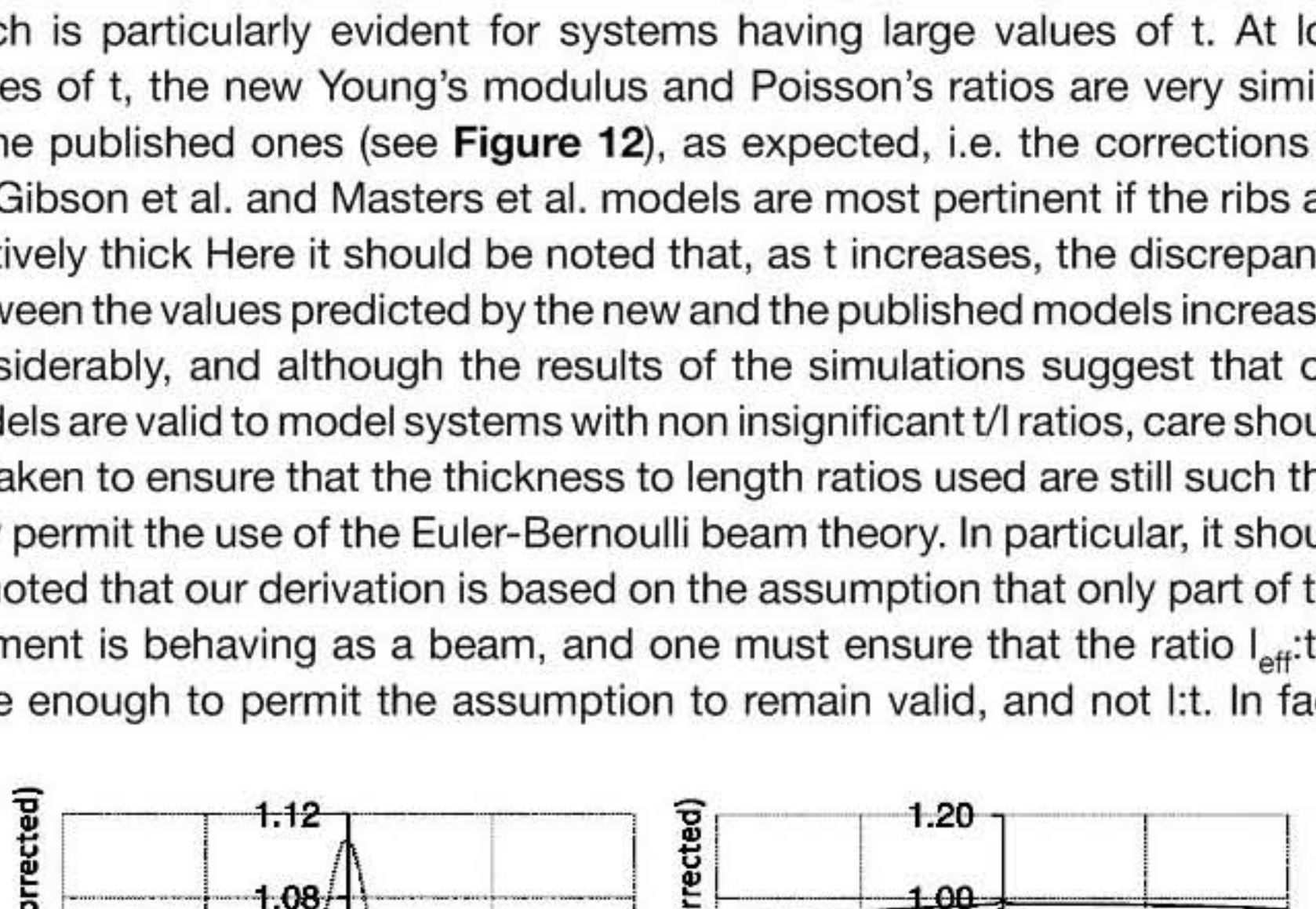

Figure 12. *Plots showing the variation of the ratio of the Poisson's ratio and Young's moduli of the idealised and corrected model as a function of θ. In the cases considered, h=20 mm and l=10 mm*

it should be highlighted that this ratio is dependent on the value of θ and although l:t remains unchanged, l_{eff}:t changes significantly with θ particularly at larger magnitudes of θ. Obviously, in such cases, the inability of the published idealised analytical model to accurately predict the mechanical properties would be even more evident, although it is expected that at larger angles and/or higher thickness values, even the corrected equations will no longer apply.

Before concluding, it is important to note that the expressions derived here are particularly important when predicting the properties of cellular nano or microstructures, in particular foam materials. For example, if one looks at typical images of foam like materials (see **Figure 13**), one will note that the t:l ratio is of an order that merits the use of the newly proposed models. Furthermore, it should be noted that in such foams, the joints usually make up a higher proportion of the cellular structure than in the ordinary honeycombs described here due to the curvature of the ligaments at the joints. Thus, the joints take up a larger fraction of the 'ligament' than what is used here for deriving the expressions for the effective corrections with the result that an even shorter effective length may need to be used. However, it should also be remembered that real materials such as foams are significantly more complex than the simple 2D model being proposed here, which at the very best may only be described by a particular 2D projection of the more complex 3D cellular structure. Nevertheless, in view of the high t/l values in such materials, it is hoped that the concepts based on what is discussed here will be incorporated in future analytical modelling of foam and similar materials.

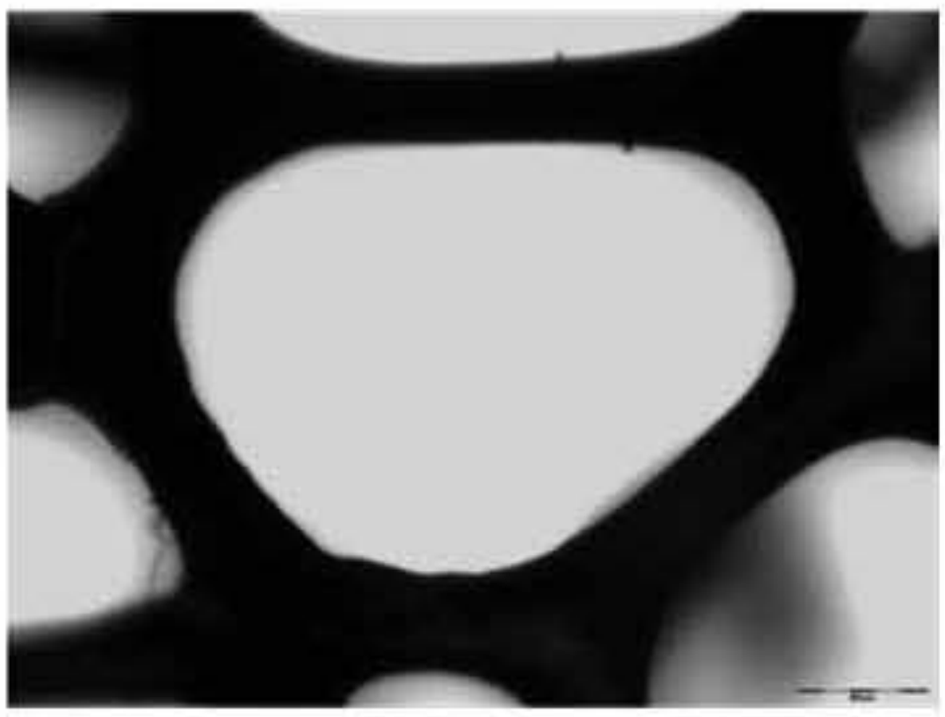

Figure 13. *The structure of a typical cell in an open cell foam having 20 ppi. Note how the material is mostly concentrated at the joints and how because of this mass of material the joints are very unlikely to deform appreciably do that most deformations occur only in a region of ribs whose aspect ratio is more accurately described by the modified model derived here*

CONCLUSION

In this work, we have shown that the mechanical properties of hexagonal honeycombs are highly affected by the thickness of the ribs and that existing analytical models need to be corrected to account for this observation. A new model has been proposed where the dimensions of the ribs are measured differently, which model requires the use of shorter values for the geometric parameters l and h. The newly proposed equations were found to offer a significantly better agreement with results of more realistic FE simulations and are likely to be more suitable to model realistic systems and may be more adequate for predicting the properties of real cellular materials having honeycomb-like nano or microstructures.

ACKNOWLEDGMENTS

The financial support of the Malta Council for Science and Technology through their 2008 R&I scheme is gratefully acknowledged as is the support of Methode Electronics (Malta) Ltd. who are partners in this project. The authors also thank the University of Malta and the Government of Malta for the financial support through a Malta Government Scholarship Scheme (Grant Number ME 367/07/17) awarded to Daphne Attard. The help of Professor Mario Valentino and Roberto Caruana Gauci of the University of Malta for recording the images of the foams used in Figure 13 is also gratefully acknowledged as is the support of Crest Foam Industries, Inc., Moonachie, NJ, for providing us with the samples of the foams.

REFERENCES

1. L.J. Gibson and M.F. Ashby, Cellular Solids: Structure and Properties (2nd ed.), Cambridge University Press, UK, 1997.

2. R. Lakes, Foam structures with a negative Poisson's ratio, *Science*, **235** (1987) 1038-1040.

3. J.N. Grima, D. Attard, R. Gatt and R.N. Cassar, A Novel Process for the Manufacture of Auxetic Foams and for Their re-Conversion to Conventional Form, *Advanced Engineering Materials*, **11** (2009) 533-535.

4. A. Alderson, K.L. Alderson, P.J. Davies and G.M. Smart, Process for the preparaation of auxetic foams, US 2010/0029796.

5. N. Chan and K.E. Evans, Microscopic examination of the microstructure and deformation of conventional and auxetic foams, *Journal of Materials Science*, **32** (1997) 5725-5736.

6. N. Chan and K.E. Evans, The mechanical properties of conventional and auxetic foams Part I:Compression and tension, *Journal of Cellular Plastics*, **35** (1999) 130-165.

7. M. Bianchi, F.L. Scarpa and C.W. Smith, Stiffness and energy dissipation in polyurethane auxetic foams, *Journal of Materials Science*, **43** (2008) 5851-5860.

8. S.A. McDonald, N. Ravirala, P.J. Withers and A. Alderson, In situ three-dimensional X-ray microtomography of an auxetic foam under tension, *Scripta Materialia*, **60** (2009) 232-235.

9. M. Bianchi, F. Scarpa, C.W. Smith and G.R. Whittell, Physical and thermal effects on the shape memory behaviour of auxetic open cell foams, *Journal of Materials Science*, **45** (2010) 341-347.

10. M. Bianchi, F. Scarpa and C.W. Smith, Shape memory behaviour in auxetic foams: Mechanical properties, *Acta Materialia*, **58** (2010) 858-865.

11. F.K. Abd el-Sayed, R. Jones and I.W. Burgens, *Composites,* **10** (1979) 209.

12. L.J. Gibson, M.F. Ashby, G.S. Schajer and C.I. Robertson, The mechanics of two-dimensional cellular materials, *Proc. R. Soc. Lond. A*, **382** (1982) 25.

13. I.G. Masters and K.E. Evans, Models for the elastic deformation of honeycombs, *Composite Structures*, **35** (1996) 403.

14. K.E. Evans, A. Alderson and F.R. Christian, Auxetic two-dimensional polymer networks: An example of tailoring Geometry for specific mechanical properties, *J. Chem. Soc. Faraday Trans.*, **91** (2005) 2671.

15. K.E. Evans, M.A. Nkansah, I.J. Hutchinson and S.C. Rogers, Molecular network design, *Nature*, **353** (1991) 124.

16. M.A Nkansah, K.E. Evans and I.J. Hutchinson, Modelling the mechanical properties of an auxetic molecular network, *Modelling and Simulation in Materials Science and Engineering*, **2** (1994) 337-352.

17. A. Bezazi, F. Scarpa and C. Remillat, A novel centresymmetric honeycomb composite structure, *Composite Structures*, **71** (2005) 356.

18. C. Lira, P. Innocenti and F. Scarpa, Transverse elastic shear of auxetic multi re-entrant honeycombs, *Composite Structures*, **90** (2009) 314.

19. K.E. Evans, M.A. Nkansah and I.J. Hutchinson, Auxetic foams: Modelling negative Poisson's ratios, *Acta Metallurgica et Materialia*, **42** (1994) 1289-1294.

20. R.F. Almgren, An isotropic three-dimensional structure with a Poisson's ratio = -1, *Journal of Elasticity*, **15** (1985) 427.

21. U.D. Larsen, O. Sigmund, S. Bouwstra, Design and fabrication of compliant micromechanisms and structures with negative Poisson's ratio, *MEMS'96 Proceedings*, (1996) 365.

22. C.W. Smith, J.N. Grima and K.E. Evans, A novel mechanism for generating auxetic behaviour in reticulated foams: Missing rib foam model, *Acta Materialia*, **48** (2000) 4349-4356.

23. J.N. Grima, R. Gatt, A. Alderson, K.E. Evans, On the potential of connected stars as auxetic systems, *Molecular Simulations*, **31** (2005) 925.

24. D. Prall, R.S. Lakes, Properties of a chiral honeycomb with a Poisson's ratio of -1, *International Journal of Mechanical Sciences*, **39** (1997) 305.

25. O. Sigmund, S. Torquato, I.A. Aksay, On th design of 1-3 Piezo-composites using topology optimisation, *J. Mater. Res.*, **13** (1998) 1038.

26. A. Alderson, K.L. Alderson, D. Attard, K.E. Evans, R. Gatt, J.N. Grima, W. Miller, N. Ravirala, C.W. Smith and K. Zied, Elastic constants of 3-, 4-and 6-connected chiral and anti-chiral honeycombs subject to uniaxial in-plane loading, *Composites Science and Technology*, **70** (2010) 1042-1048.

27. R. Lakes, Deformation mechanisms in negative Poisson ratio materials - structural aspects, *J. Mater. Sci.*, **26** (1991) 2287.

28. H. Tanaka, Y. Shibutani, In-plane mechanical behaviours of 2D repetitive frameworks with four-coordinate flexible joints and elbowed beam members, *Journal of the Mechanics and Physics of Solids*, **57** (2009) 1485.

29. N. Chan and K.E. Evans, Indentation resilience of conventional and auxetic foams, *Journal of Cellular Plastics*, **34** (1998) 231-260.

30. C.W. Smith, F. Lehman, R.J. Wootton and K.E. Evans, Strain dependent densification during indentation in auxetic foams, *Cellular Polymers*, **18** (1999) 79-101.

31. A. Bezazi and F. Scarpa, Tensile fatigue of conventional and negative Poisson's ratio open cell PU foams, *International Journal of Fatigue*, **31** (2009) 488-494.

32. F. Scarpa and G. Tomlinson, Theoretical characteristics of the vibration of sandwich plates with in-plane negative Poisson's ratio values, *Journal of Sound and Vibration*, **230** (2000) 45-67.

33. F. Scarpa, L.G. Ciffo and J.R. Yates, Dynamic properties of high structural integrity auxetic open cell foam, *Smart Materials and Structures*, **13** (2004) 49-56.

34. F. Scarpa, P. Pastorino, A. Garelli, S. Patsias and M. Ruzzene , Auxetic compliant flexible PU foams: static and dynamic properties, *Physica Status Solidi B*, **242** (2005) 681-694.

35. A. Bezazi and F. Scarpa, Mechanical behaviour of conventional and negative Poisson's ratio thermoplastic polyurethane foams under compressive cyclic loading, *International Journal of Fatigue*, **29** (2007) 922-930.

36. A. Alderson, J. Rasburn and K.E. Evans, Mass transport properties of auxetic (negative Poisson's ratio) foams, *Physica Status Solidi B*, **244** (2007) 817-827.

37. K.R. Olympio and F. Gandhi, Zero Poisson's Ratio Cellular Honeycombs for Flex Skins Undergoing One-Dimensional Morphing, ***Journal of Intelligent Material Systems***, **21** (2010) 1737-1753.

38. D. Attard and J.N. Grima, Modelling of hexagonal honeycombs exhibiting zero Poisson's ratio, ***Physica Status Solidi B***, **248** (2011) 52-59.

39. J.N. Grima, R. Gatt, P.S. Farrugia, On the properties of auxetic meta-tetrachiral structures, *Phys. Stat. Sol. (b)* 2008, **245**, 511.

40. R.J. Roark and W.C. Young, Formulas for Stress and Strain, 5th ed., McGraw-Hill, London, 1976.